THERMAL STRESS-INDUCED MICROCRACKING IN BUILDING GRANITE

Freire-Lista, D.M.[a,b,*], Fort, R.[a,b], Varas-Muriel, M.J.[a,b,c]

[a]*Instituto de Geociencias IGEO (CSIC, UCM) Spanish Research Council CSIC – Complutense University of Madrid UCM. Madrid 28040, Spain*
[b]*CEI Campus Moncloa, UCM-UPM and CSIC, Madrid 28040, Spain*
[c]*Facultad de CC. Geológicas. Complutense University of Madrid UCM. Madrid, 28040, Spain*

*Corresponding author.
E-mail addresses: d.freire@igeo.ucm-csic.es

Abstract

Microcracking induced by wide fluctuations in temperature affects granite quality and durability, making the stone more vulnerable to decay. Determining the extent of that effect is not always straightforward, however, given the excellent durability of these materials.

Four types of construction granite quarried in the region of Madrid, Spain, and frequently used in both the built heritage and in de novo construction (Alpedrete, Cadalso de los Vidrios, Colmenar Viejo and Zarzalejo) were exposed to 42 thermal cycles (105-20º C; UNE-EN, 14066, 2003). Petrographic and petrophysical properties were analysed using both destructive and non-destructive techniques. Microcracking generated in the granite stones by 42 thermal cycles had barely any impact on their petrophysical properties, which are the parameters normally assessed to establish material quality and durability. Their petrographic properties, which are not generally assessed in this type of studies, were affected, however. This study contends that petrographic analysis is needed to objectively quantify the actual quality and durability of the most highly resistant materials when petrophysical studies are inconclusive. Petrographic and fluorescence microscopy, along with fractography, are among the most prominent techniques for petrographic exploration. Thanks to the deployment of these techniques, mineral microcracking could be monitored throughout the present tests conducted.

The microscopic findings revealed substantial micro-textural and microstructural change in and around the granite minerals, which play a prominent role in decay. The findings showed that pre-existing microcracks coalesced and generated further microcracking as decay progressed. Microcracking was most intense in Zarzalejo granite due to its textural characteristics determined by its high feldspar content. Microscopic observation revealed that the microstructure of feldspar minerals, with their crystallographic anisotropies and secondary mineral phases, favoured microcrack development. Zarzalejo granite exhibited lower quality and durability than Colmenar Viejo and Cadalso de los Vidrios granites, which were more resistant to heat treatment.

Keywords: granite, microcracks, petrography, petrophysics, decay.

1 Introduction

The granite in historic and contemporary buildings is exposed to thermal changes that may induce stone decay. When thermal stress is high and the material is unable to adapt quickly enough to accommodate the strain generated during cooling, microcracks appear due to differences in the expansion coefficients between constituent minerals or even within the same mineral (Hall, 1999; Hale and Shakoor, 2003; Yavuz, 2011; Demirdag, 2013). The effects of thermal changes on granite have been studied by a number of authors (Heuze, 1983; Homand-Etienne and Troalen, 1984; Homand-Etienne and Houpert, 1989; Iñigo et al., 1999, 2013; Sousa., 2005, Nasseri, et at., 2007; Takarli, et al., 2008) in experiments in which temperatures and number of heating cycles differed. The temperatures generating stone decay range widely: granite exposed to heating-cooling cycles over a range of 30 °C to 80 °C exhibited significant decay (Gräf et al., 2013). Lin (2002) established a threshold temperature of 100 °C to 125º C for microcracking in Inada granite.

The procedure described in Spanish and European standard UNE-EN 14066, 2003 for accelerated ageing in natural stone calls for heating the material to 105 °C in air followed by cooling in water to 20 °C.

Exposing the stone to such temperatures at short (24 h) cycles simulates the effects of fire extinction (Pires et al., 2014; Mambou et al., 2015), indoor heating, abrupt cooling by frequent rain after intense solar radiation (tropics) or the significant differences in day and night time temperatures in desert climates, such as found in the Middle East and certain continental regions of Asia, Australia, Europe and the United States (Erguler and Shakoor, 2009).

To ensure high performance under any circumstances, building stone must meet high quality standards (Siegesmund and Török, 2011). Such performance is normally determined on the grounds of petrophysical properties and mechanical strength (UNE-EN 771-6, 2012).

This study determined the thermal effect of accelerated ageing as specified in Spanish and European standard UNE-EN 14066, 2003 on four types of granite widely used in heritage construction on the Iberian Peninsula and more recently in other areas of the world (Freire-Lista et al., 2015a, b, c, d; Freire-Lista and Fort, 2015). This study aimed primarily to establish a new analytical method for ascertaining the quality and durability of building stones exposed to variations in temperature when their petrophysical properties remain largely unaffected. That method is based on assessing variations in their petrographic properties.

The assessment of the physical and mechanical properties of building stone has been amply addressed in the literature (Dearman et al., 1978; Fort et al., 2010, 1011, Siegesmund and Dürrast, 2011). These studies examine fundamental properties such as apparent density and porosity (Benavente et al., 2004). Other trials that furnish information on ultrasonic wave velocity, Young's modulus, colour and surface hardness are imperative to predicting stone performance under environmental conditions that may drastically reduce its service life (Smith and Prikryl, 2007). Such trials are also essential in restoration studies prior to or conducting stability analyses on, conserving or cleaning granite structures.

Despite the significant role of petrographic properties such as particle size and shape and microstructural features such as microcracks (Tuğrul et al., 1999, 2004; Seo et al., 2002; Upadhyay, 2012; Sousa 2013; Sajid et al., 2016),in the long-term behaviour of granite, very little research has been conducted on these parameters under varying construction and environmental conditions.

As thermally induced propagation of microcracks (Alm et al., 1985; Taboada and García, 1999; Iñigo et al., 2000, Akesson et al., 2003, Nasseri et al., 2007; Anders et al., 2014) affects the constituent minerals in granite differently (Miskovsky et al., 2004), it may cause physical and chemical changes in the internal texture of the stone, associated on occasion with changes in its physical and mechanical properties (Kern et al., 1997; Tuğrul, 2004; Schubnel et al., 2006). Microcrack propagation and stone colour change (Ozcelik et al., 2012) are the most common symptoms of thermally induced decay.

Since granite massifs are regarded, worldwide, as a reservoir of suitable building stone, granite durability and its determination are a major concern when choosing a construction material (Sousa et al., 2005; Chaki et al., 2008; Dwivedi et al., 2008; Takarli et al., 2008; Wanne and Young, 2008; Franzoni et al., 2013; and Shao et al., 2014). Microcrack coalescence and the thermally induced generation of further cracking induces decay in building granite that may be intensified by the action of other agents of decay, such as lichen colonies (De la Torre et al., 2010, Scarciglia et al., 2012), pollution-related grime (Schiavonma, et al., 1995) and graffiti (Rivas et al., 2012).

2 Materials and methods

The decay caused by the thermal treatment test was monitored in four types of granite building stones with nine analytical techniques: effective porosity (*Pe*), bulk density (*ρb*) ultrasonic pulse velocity P (V_p) and S (V_s), dynamic Young's modulus (E_{dyn}), mercury intrusion porosimetry (MIP), surface hardness (*L*), spectrophotometry and microcracking calculating linear crack density (LCD).

2.1 Rock samples

The Spanish Central System comprises primarily Variscan granitoids (344 Ma to 285 Ma; Villaseca et al, 2012). The stone forming the Sierra de Guadarrama, located on the northeastern edge of the system, includes four major types of monzogranite: biotitic monzogranites containing some cordierite, biotitic monzogranites containing some amphibole, biotitic monzogranites with no cordierite or amphibole, and leucogranites (see Figure 1).

The four monzo- and leucogranite stones selected for this study, Alpedrete (AL), Cadalso de los Vídrios (CA), Colmenar Viejo (CO) and Zarzalejo (ZA) (Figure 2), were quarried in the Sierra de Guadarrama (Spanish Central System). These stones, popularly called ‘Piedra Berroqueña’, have been traditionally used in construction in Madrid and surrounds (Gómez-Moreno et al., 1995; Fort et al., 2013; Freire-Lista et al., 2015b, c; Freire-Lista and Fort, 2015), where they are still used today, while some are also exported for construction.

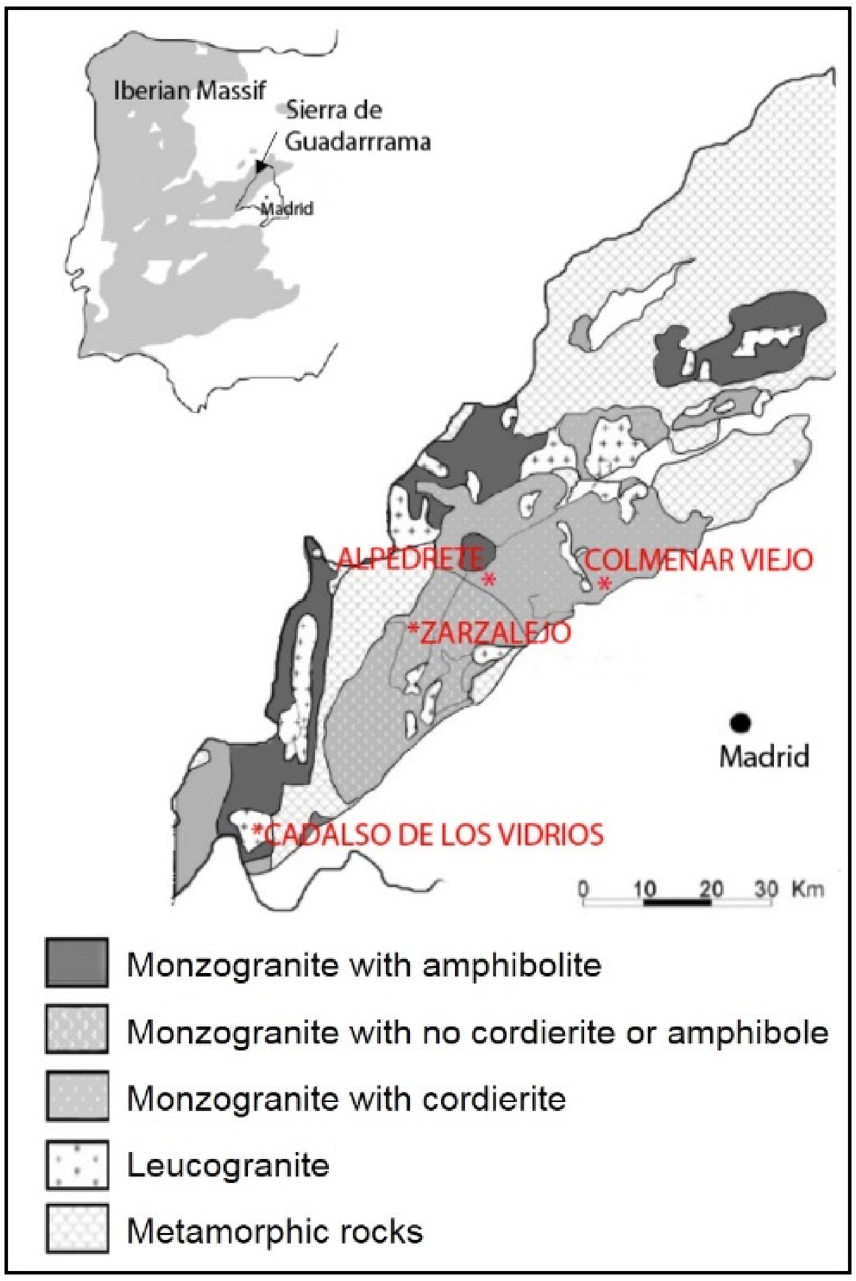

Fig. 1. Site map for Alpedrete, Cadalso de los Vidrios, Colmenar Viejo and Zarzalejo granites

Fresh, poorly fractured blocks located far from fault systems were selected from four outcrops close to the old quarries and extracted along the quarry orientation. Quarry locations are shown in Figure 1. Following extraction, seven cubic (5 × 5 × 5 ± 0.5 cm) specimens of each of the four types of granite were cut at low speed (120 rpm) and low strain. Surface areas were rejected to minimise the effect of possible extraction-induced cracking. No fissures were visible in any of the samples tested.

AL, a medium-grained, hypidiomorphic, equigranular monzogranite with cordierite, has been used in the construction of prominent heritage buildings, including the Royal Palace (1738-1764) and the Puerta de Alcala (1770-1778) in Madrid. This granite has been nominated as a 'Global Heritage Stone Resource' (Freire-Lista et al., 2015b) for its significance in the built heritage.

CA, a fine-to-medium-grained hypidiomorphic, equigranular leucogranite (González-Casado et al., 1996), can be seen on heritage buildings such as the Palacio de Villena (15^{th} century). Much more recently, under the trade name Blanco Cristal, it has been used in places such as Cork Airport in Ireland, and shopping centres in China (Guangzhou, Shanghai).

CO is a medium-to coarse-grained, heterogranular monzogranite with no cordierite or amphibolite. It has been found in archaeological sites dating from the 6^{th} to the 7^{th} century and forms part of much more recent structures, including prominent government buildings such as the Nuevos Ministerios complex in Madrid (1933-1942).

ZA is a coarse-grained, hypidiomorphic, heterogranular monzogranite with no cordierite or amphibolite, used in historic construction (San Lorenzo de El Escorial Royal Monastery outside Madrid, 1563-1584), restoration (Royal Palace, 1945), as well as in modern building (shopping centres, enlargement of the Reina Sofia Museum, 2001-2005) in Madrid. Nominated as a 'Global Heritage Stone'", this granite is presently exported, mainly in blocks, to Turkey and Italy.

The four regions from which the samples were extracted exhibit a similar tectonic history (De Vicente et al., 2007; Mejías et al., 2009; Villaseca et al., 2012). The four types of granite share a similar mineralogy (quartz, plagioclase, K-feldspar and biotite) (Figure 2) and their crystal size, in ascending order, is CA<AL<CO<ZA. Isotopic data suggest that they derived from similar sources (Vilaseca 2012). Some areas of the Guadarrama Mountains are characterised by Lower Permian regional hydrothermal processes (Caballero, et al., 1996; Mejías et al., 2009). The granite quarried was taken from areas with no signs of hydrothermal damage.

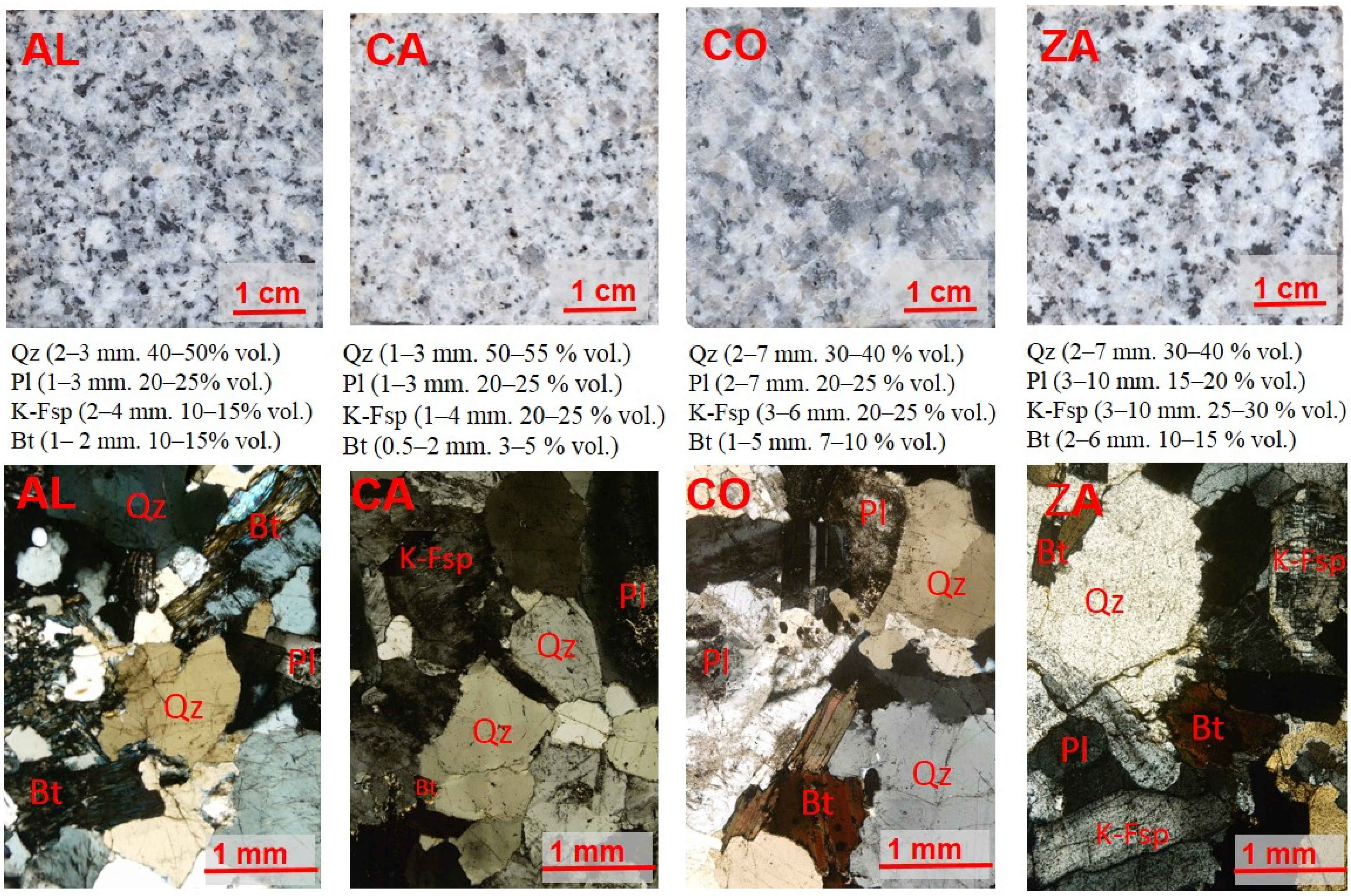

Fig. 2. Alpedrete granite (AL), Cadalso de los Vidríos granite (CA), Colmenar Viejo granite (CO) and Zarzalejo granite (ZA); above: hand samples; below: crossed Nicol microscopic images

2.2 Thermal cycles

Seven cubes of each granite were subjected to thermal cycles lasting 24 hours (UNE-EN, 14066, 2003). The samples were first placed in an oven at 105 ± 5º C for 18 hours, then immersed in water at 20 ºC for 6 hours. This cycle was repeated 42 times.

2.3 Effective porosity (Pe)

To obtain information on the number of microcracks generated during the thermal cycles, Pe was found before and after 42 thermal cycles.

The granite samples were tested for this parameter using the natural stone method described in Spanish and European standard UNE-EN 1936, 2007. After the granite samples had reached a constant weight, they were placed in a vacuum chamber at 2 kPa for 2 hours, then slowly submerged in water (room temperature) and soaked at atmospheric pressure for 24 hours to induce water saturation. The Pe values were calculated from Equation (1)

$$Pe\ (\%) = ((Ws-Wd)/(Ws-Wh)) \times 100 \quad (\%) \qquad (1)$$

Where Ws is the weight of the 24 hour water-saturated sample, Wd is the dry weight of the sample and Wh is the weight of the sample submerged in water.

Weight rises in the post-test water-saturated samples denote higher sample porosity, an indication of microcracking. Hydric properties such as Pe and ρb are indicative of granite resistance to water, one of the major agents of decay in buildings (García-del-Cura et al., 2008).

2.4 Bulk density (ρb)

Bulk density (ρb) was found further to Spanish and European standard UNE-EN 1936, 2007 as the ratio between specimen mass and its bulk volume, from equation (2):

$$\rho b\ (kg / m^3) = ((Wd) / (Ws-Wh)) \times 1000\ kg / m^3 \qquad (2)$$

This parameter furnishes information on the microcracks generated during thermal cycles (Shao et al., 2014; Sousa, 2014). Small variations are construed to mean only minor microcracking.

2.5 Ultrasonic pulse velocity (V_p and V_s)

V_p ultrasonic pulse measurements were taken on a CNS Electronics PUNDIT analyser (precision: ±0.1 µs) pursuant to Spanish and European standard UNE-EN, 14579, 2007. One MHz transducers (11.82 mm in diameter) were attached to the granite surface with Henkel Sichozell Kleister (a carboxymethyl cellulose) paste and water to enhance the transducer-stone contact.

V_p was measured on four cubes of each granite in the three orthogonal directions, using the mean of four consecutive measurements on each face of the cube as the accepted value. V_p was determined before and after the 42 thermal cycles.

A Panametrics High Voltage pulser-receiver (Model 5 058 PR) connected to a Tektronix digital phosphorous oscilloscope (Model TDS 3 012 B) was used to measure the V_s ultrasonic pulse.

Round, smooth (Panametrics V151, 25.4 mm in diameter) 0.5 MHz transducers were affixed to the granite sample surfaces with a coupling gel consisting in 80 % sugar (primarily fructose and glucose) and about 20 % water to enhance the transducer-stone contact and bond. The test conditions were: pulse repetition rate, 20 Hz and damping, 200 Ω.
V_s was measured once on each face of the seven samples of the four granites, i.e., in the three orthogonal directions, using the mean V_s reading taken in the three axes of each cubic specimen of each granite as the accepted value. V_s was determined before and after the 42 thermal cycles

Ultrasonic pulse velocity provides an accurate measurement of total decay in granite exposed to thermal processes (Reuschlé et al., 2006). It has been used to characterise thermal microcracking in rock and predict the degree of granite weathering (Fredrich and Wong, 1986; Chen et al., 2008; Gokceoglu et al., 2009; Inserra et al., 2013). Slower ultrasonic P-wave (V_p) and S-wave pulse (V_s) velocity denotes microcrack generation. Given the portability of this non-destructive technique, granites can be compared in situ to establish reference values.

2.6 Young's modulus (*E*)

Weathering-induced changes in the form of internal microcracks often invisible on the surface can be identified with the aid of mechanical modules (Moses et al., 2014). Young’s modulus is conventionally determined with destructive tests (Takarli and Prince-Agbodjan, 2008). In historic buildings it is not always possible to test mechanical strength directly, for it involves breaking the specimens. In such cases the dynamic modulus must be obtained using non-destructive techniques (Christaras et al., 1994; Murphy et al., 1996; Svahn, 2006; Brotóns et al., 2013)

V_p and V_s values were used to compute the Young´s dynamic modulus (E_{dyn}), as per Darracott and Orr (1976) (Eq. (3)). The V_p/V_s ratio was also found.

$$E_{dyn}=\rho b\ [3\ V_p^2-4V_s]/[(V_p/V_s)^2-1] \qquad (3)$$

Where: V_p is ultrasonic P-wave pulse velocity (m/s) and V_s the ultrasonic S-wave pulse velocity (m/s); E_{dyn} is Young´s dynamic modulus (MPa); and ρb is bulk density (kg/m^3). Declines in E_{dyn} denote structural alteration associated with a rise in weathering-induced microcracking (Vasconcelos et al., 2007, 2009). The Young's modulus values given in this paper were obtained for each granite studied before and after the thermal cycles. E_{dyn} represents the experimental data compiled and needed as input in advanced non-linear numerical analysis of granite members in heritage structures.

2.7 Mercury intrusion porosimetry (MIP)

MIP was studied on a single prismatic specimen (12 ± 2 mm in diameter and 20 ± 2 mm high) cut from an upper corner of one of the cubic granite specimens. The analysis was run before and after 42 cycles on samples oven-dried at 70 °C to a constant weight. This test was conducted to obtain information on microcrack size. Pore distribution, defined as macropores (diameter >5 µm) and micropores (diameter < 5 µm), was determined on a Micromeritics Autopore IV 9520 porosimeter (maximum pressure, 414 MPa (60 000 psi); pore throat diameter measuring range 0.001 µm to 400 µm) (Russel, 1927; Rodríguez and Sebastián, 1994; Fort et al., 2011).

2.8 Surface hardness (*L*)

Prior to the thermal test, four cubes, each cut from the four granites, were dried to a constant weight. Surface hardness was measured before and after the thermal test on an Equotip 3 (D) electronic rebound hardness testing electronic device (Kawasaki et al., 2002; Aoki and Matsukura, 2007, 2008; Viles et al., 2011), with an impact energy of 11 N mm to prevent the impact from affecting the samples. This tester has been used to measure the effects of weathering on rock hardness (Verwaal and Mulder, 1993; Kawasaki and Kaneko, 2004). Ten measurements were performed on each face of the samples (6 × 25 cm^2). The instrument was held vertically face down and perpendicular to the flat surface within 5 mm of the edge of the cube to avoid edge effects and care was taken not to select testing points close to the vicinity of voids visible on the rock surface.
A total of 60 hardness measurements per sample were taken and an average was calculated for each type of granite. The hardness value was expressed as the Leeb number (*L* value), which is the ratio of the rebound velocity at impact velocity multiplied by 1000. *L* values are interpreted to be indicative of rock strength (Viles et al., 2011).This is a particularly significant property in building granite, in which lower surface hardness may lead to colonisation by microorganisms and pose cleaning problems.

2.9 Colour

Colour change is a common type of decay in granite exposed to thermal stress (Gómez-Heras, 2006a; Vázquez, 2010; Iñigo et al., 2013). Colour change was measured on a Minolta CM-700d / 600D with a CM-S100 W COLOR DATA Software SpectraMagic NX spectrophotometer. Once each cubic sample had reached a constant mass, 10 colour measurements were taken on each face of the cubic specimens. Measurements were averaged for each granite.

The CIELAB system (CIELAB, 1976) colour parameters were used: luminosity (L *), red to green coordinate (a *) and blue to yellow coordinate (b *). The Spanish and European standard UNE-EN 15886, 2011 yellow (YI *) and white (WI *) indices as well as overall colour change (AE *) were also obtained.

Colour variation in the samples before and after the thermal test was numerically compared on the grounds of the overall colour change, $\Delta E^*=\sqrt{(\Delta L^*)^2 + (\Delta a^*)^2 + (\Delta b^*)^2}$.

2.10 Microscopy and Fractography

Petrographic (PM) and fluorescence (FM) microscopy to determine rock texture and composition are essential to identifying the early development of microcracks generated by the thermal test. Sousa et al. (2005) used these techniques to quantify and assess microcracks in ornamental granite.

A 30 × 20 ± 3 mm thin section measuring 30 µm thick was sectioned from one specimen each of the AL, CA, CO and ZA granites before thermal testing and after 21 and 42 cycles. These thin sections were cut from the exposed parallel faces of the specimens to ensure that the microcrack propagation observed involved cracks running in the same direction.

Sawing was performed at a low speed (120 rpm) and a low strain so as not to generate microcracks. All thin sections were impregnated with fluorescence and characterised under an Olympus BX 51 polarized light microscope (PM) fitted with a DP 12-coupled (6 V/2.5 Å) Olympus digital camera and Olympus DP-Soft software (version 3.2). Microcracks were characterised with the same instrument, as well as with the same set-up using an Olympus U-RF-T mercury lamp fluorescence microscope (FM).

Micrographs were taken to study the microcracks (Laubach, 1997; Åkesson et al., 2004; Gale et al., 2010).
PM and FM micrograph mosaics were generated for nearly all the thin sections to monitor microcrack development during the thermal cycles and ensure that the microcrack count was representative.

Each mosaic comprised 40 micrographs from the same 4.5 cm^2 area. The cross-Nicols micrograph mosaics were used for mineral quantification and the fluorescence mosaics to study microcracks.

The FM micromosaic was overlaid on the PM micromosaic to establish a 1×2 cm network divided into 5×5 mm squares (linearly, a total of 110 mm). The sides of this network were drawn parallel to the two sides of the original thermally tested cubic specimen (Figure 3).

The number of microcracks intersecting with the lines defining this network were measured. Microcracks affecting quartz (Qz), potassium feldspar (K-Fsp), plagioclase (Pl) and biotite-group minerals (Bt) were classified as intracrystalline (if contained within a single crystal), intercrystalline (if between lines bordering the edges of the crystal) or trans-crystalline (if affecting more than one crystal). The number of microcracks was divided by the total length of the lines in the network (110 linear mm) to calculate the number of microcracks per linear millimetre (Linear Crack Density - LCD) Wang et al. (1989), Sousa (2005), Ismael and Hassan (2008) and Vázquez et al. (2010) successfully used LCD to count microcracks.

The response of each mineral to thermal test-induced microcracking was calculated on the grounds of the percentage of area occupied by the minerals in each granite (Figure 2). In other words, the number of microcracks in each mineral was divided by the percentage of the area occupied by this mineral in each granite.

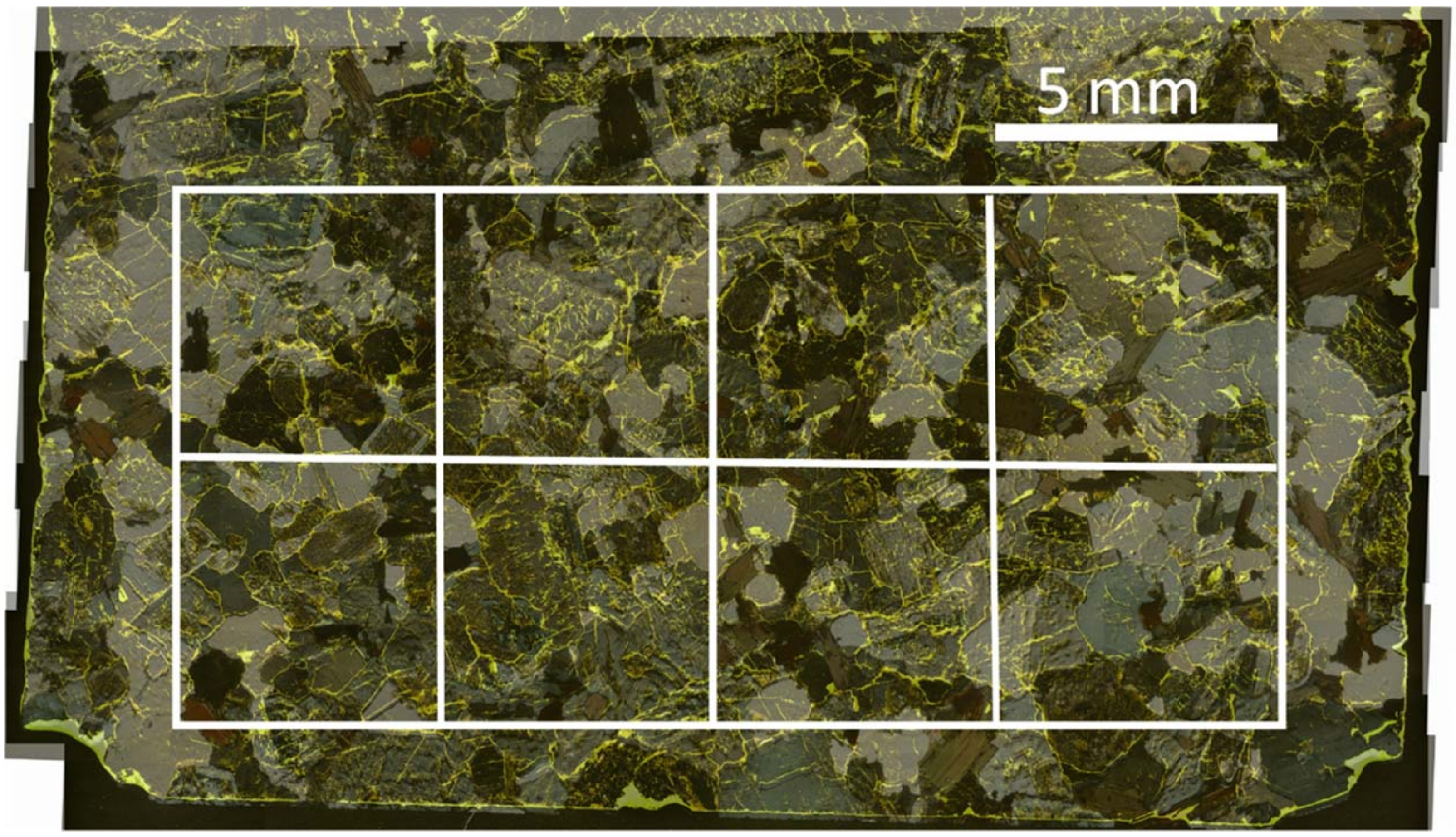

Fig. 3. Thin section of an Alpedrete granite specimen: FM micrograph mosaic overlaid on the same area of a PM micrograph mosaic (crossed Nicols) and 20×10 mm rectangle divided into 5×5 mm squares

3 Results

3.1. Petrophysical properties

Heating and subsequent water cooling affected the bulk density (*ρb*) and effective porosity (*Pe*) of the granites studied. The initial *ρb* was similar in the four granites prior to testing, ranging from 2 602 ± 16 kg/m^3 in CA to 2 668 ± 18 kg/m^3 in AL, and varied very little throughout the thermal test. The steepest decline in º*ρb* (0.3 %) was recorded for ZA, whose post-thermal test effective porosity was 1.78 %. The initial Pe was lowest in CO (0.71 %) and highest in ZA (1.72 %), with Al (0.83 %) and CA (1.21 %) exhibiting intermediate values. The pre- and post-heating Pe varied only scantly, although the sharpest rise in this parameter was observed for CO (4.2 %).

Table 1. Ultrasound wave velocity (V_p and V_s) in the four granites studied before and after 42 thermal cycles

Granite	V_p (m/s)			Vs (m/s)		
	Initial	Final	Δ(%)	Initial	Final	Δ(%)
AL	4 678 ± 172	4 396 ± 187	-6.0	3 816 ± 101	3 078 ± 151	-19.3
CA	3 694 ± 151	3 439 ± 130	-6.9	2 590 ± 108	2 294 ± 110	-11.4
CO	5 051 ± 149	4 895 ± 103	-3.1	3 489 ± 106	3 251 ± 258	-6.8
ZA	3 319 ± 104	3 084 ± 170	-7.1	2 110 ± 92	2 062 ± 113	-2.3

AL: Alpedrete granite; CA: Cadalso de los Vidrios granite; CO: Colmenar Viejo granite; ZA: Zarzalejo granite; Δ: variation

The 12 P-wave velocity measurements for the four granite specimens (means of 12 readings) are listed in Table 1.

The test findings confirmed that exposure to a temperature of 105 ºC followed by water cooling induced a decline in V_p and V_s in all four varieties of granite.

Young´s dynamic modulus (E_{dyn}) found as per Equation 3 was initially highest in CO (66 637 MPa), followed by AL (47 260 MPa), CA (34 673 MPa) and ZA (27 488 MPa). E_{dyn} declined after the 42 cycles in all four varieties of granite: --6.2 % in CO, -9.5 % in AL, -10.2 % in ZA and -13.0 % in CA. CO had the highest (623 293 MPa) and ZA the lowest (24 686 MPa) post-test E_{dyn}.

The four granites exhibited low initial MIP. Figure 4 shows the pore diameter distribution for the four granites in cycles 0 and 42 as determined by MIP. Pre- and post-heating MIP findings on the micro- and macroporosity of the granites studied are given in Table 2.

Table 2. Mercury intrusion porosimetry (MIP)-based micro- and macroporosity for the four granites studied before and after thermal testing

Granite	MIP (%)			Macroporosity (%)			Microporosity (%)		
	Initial (%)	Final (%)	Δ(%)	Initial (%)	Final (%)	Δ(%)	Initial (%)	Final (%)	Δ(%)
AL	0.4	0.7	75.0	0.1	0.3	200	0.3	0.4	33.3
CA	1.0	1.5	50.0	0.3	0.4	33.3	0.7	1.1	57.1
CO	0.5	0.6	20.0	0.3	0.2	-33.3	0.2	0.3	50.0
ZA	1.4	1.8	28.6	0.3	0.7	133.3	1.1	1.1	0

AL: Alpedrete granite; CA: Cadalso de los Vidrios granite; CO: Colmenar Viejo granite; ZA: Zarzalejo granite; Δ: variation

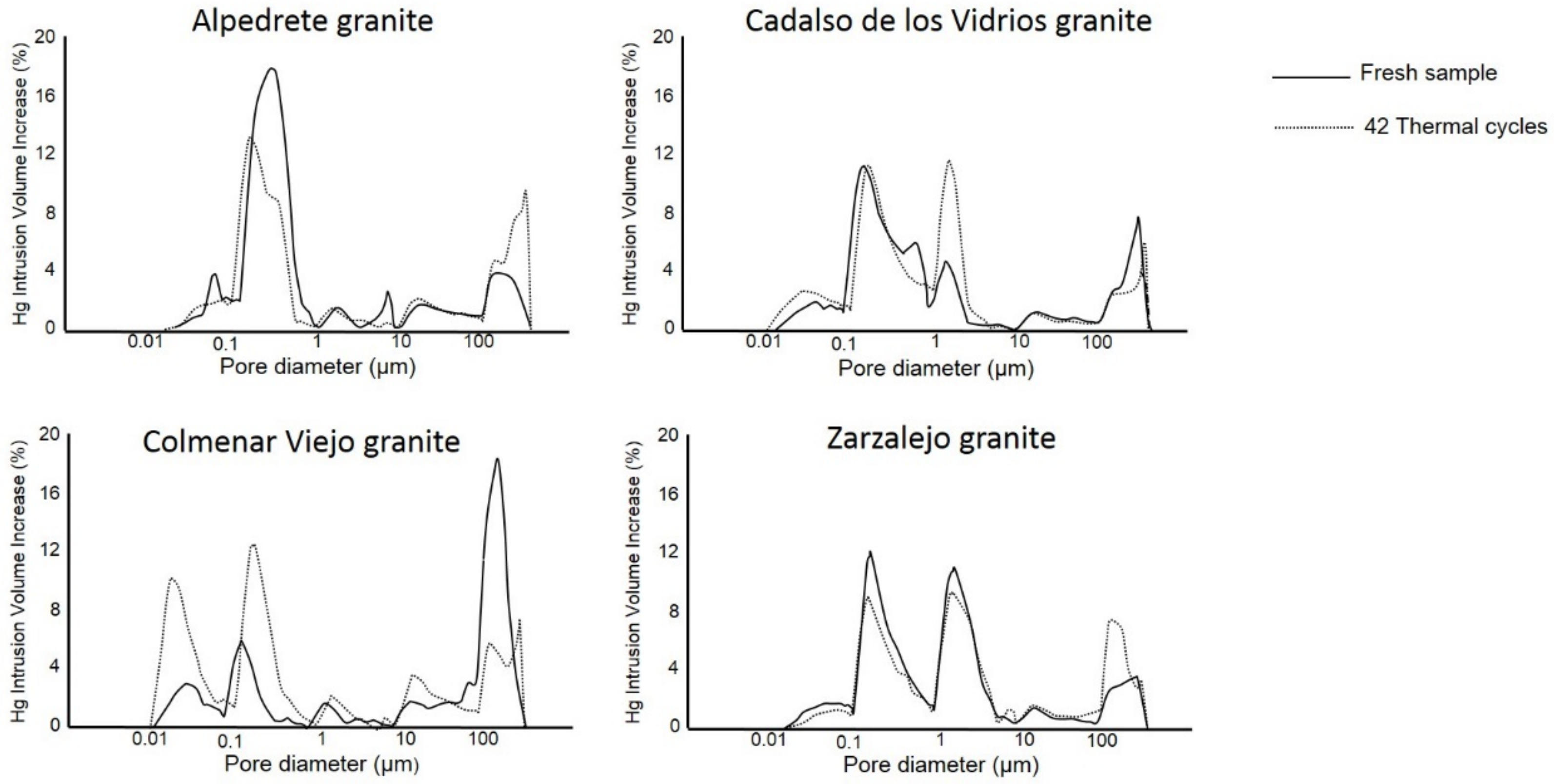

Fig. 4. Pore size distribution determined by MIP for four thermally tested granites

Further to the pre- and post thermal cycle colour measurements listed in Table 3, the four granites exhibited similar colour coordinates. This quantification denoted the existence of lightly hued, matte colours, with greyish-white tones as a result of the presence of smoke grey Qz, grey-white K-Fsp, yellowish white Pl and very few biotite-group minerals. Slight colour changes were quantified after accelerated thermal ageing.

Table 3. Colour parameters before and after 42 thermal test cycles

Granite	L*		a*		b*		YI		WI		ΔE*
	Initial	Final	Initial	Final	Initial	Final	Initial	Final	Initial	Final	
AL	68.2	70.4	-0.5	-0.6	1.0	0.1	1.7	-0.1	35.8	41.5	2.4
CA	78.8	77.6	-0.5	-0.5	2.3	2.2	4.0	3.8	46.1	44.7	1.2
CO	71.1	73.9	-0.4	-0.4	2.9	3.6	5.4	6.6	33.5	34.3	2.9
ZA	73.0	75.5	-0.3	-0.5	2.2	2.4	4.0	4.3	38.2	40.9	2.5

AL: Alpedrete granite; CA: Cadalso de los Vidrios granite; CO: Colmenar Viejo granite; ZA: Zarzalejo granite; Δ: variation; L *: lightness; a * red-green value; b *: blue-yellow value; WI: whiteness index; YI: yellowness index; $\Delta E^*=\sqrt{(\Delta L^*)^2+(\Delta a^*)^2+(\Delta b^*)^2}$: overall colour change

The four granites exhibited high initial surface hardness, which declined slightly after the 42 thermal cycles. The pre- and post-thermal test hardness data are given in Table 4.

Table 4. Surface micro-hardness (*L*) before and after 42 thermal cycles

Granite	L		
	Initial	Final	Δ (%)
AL	861	843	-2.1
CA	869	843	-3.0
CO	871	848	-2.6
ZA	802	761	-5.1

AL: Alpedrete granite; CA: Cadalso de los Vidrios granite; CO: Colmenar Viejo granite; ZA: Zarzalejo granite; Δ: variation

3.2 Fractography

The number of microcracks rose in all four granites after the thermal cycle test. The micrographs for all four stones after 0, 21 and 42 cycles are reproduced in Figure 5. Figure 6 shows the variations in granite linear crack density (LCD). CO had the smallest number of microcracks (LCD=0.7) at the outset and was the rock in which the smallest number was generated, LCD=1.3. While the largest number of pre-existing microcracks (LCD=1.4) was found for CA, this was the granite with the smallest post-test increase (Δ LCD=61 %). ZA ended the thermal test with the largest number of microcracks, at LCD=2.5, for a 96 % increase.

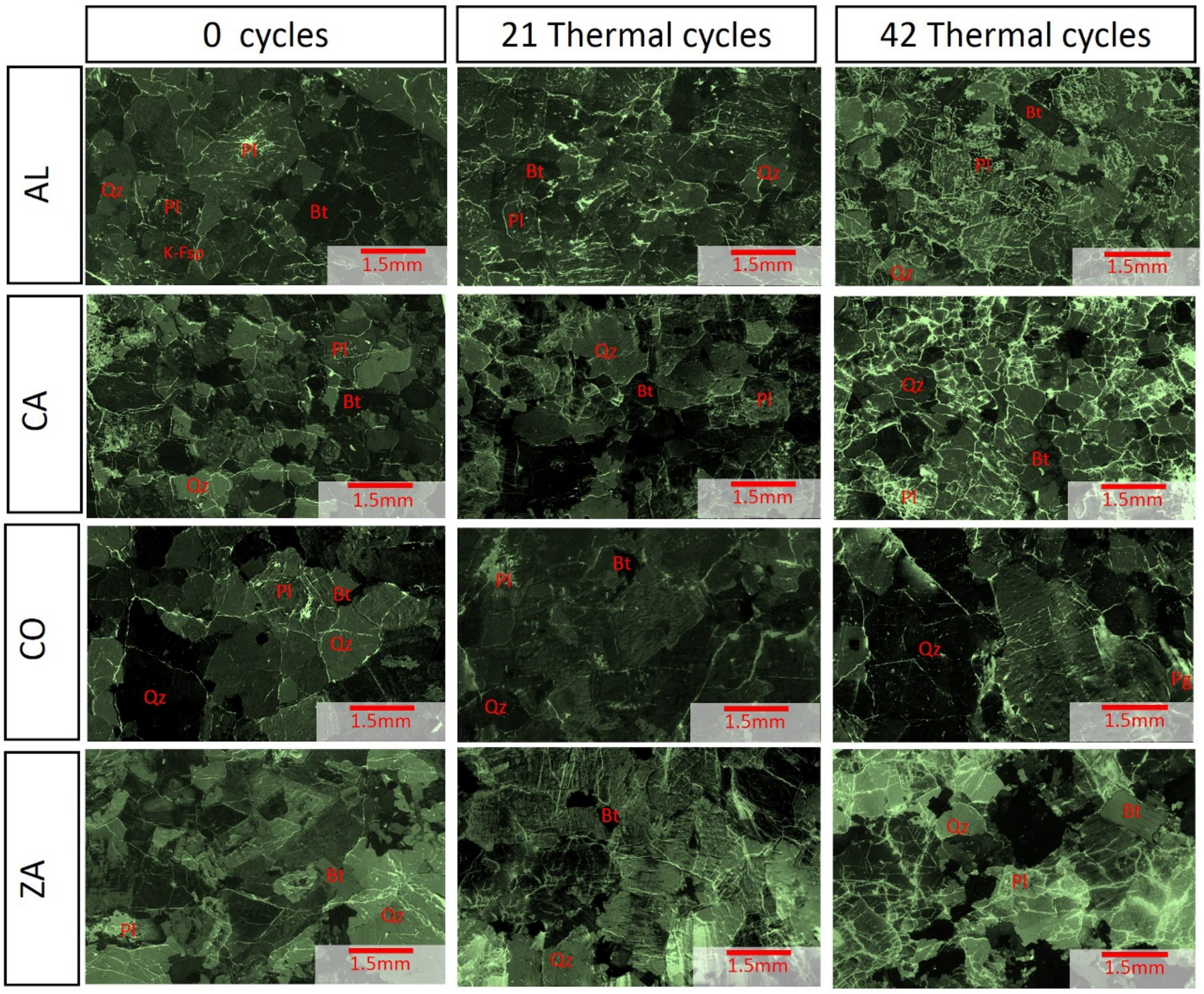

Fig. 5. Polarised petrographic (crossed Nicols) micromosaics overlaid on fluorescence micrographs; from the top down: AL: Alpedrete granite, CA: Cadalso de los Vidrios granite, CO: Colmenar Viejo granite, ZA: Zarzalejo granite; left: before thermal testing; centre after 21 cycles; right: after 42 cycles; Bt: biotite-group minerals; K-Fsp: potassium feldspar; Qz: quartz, Pl: plagioclase

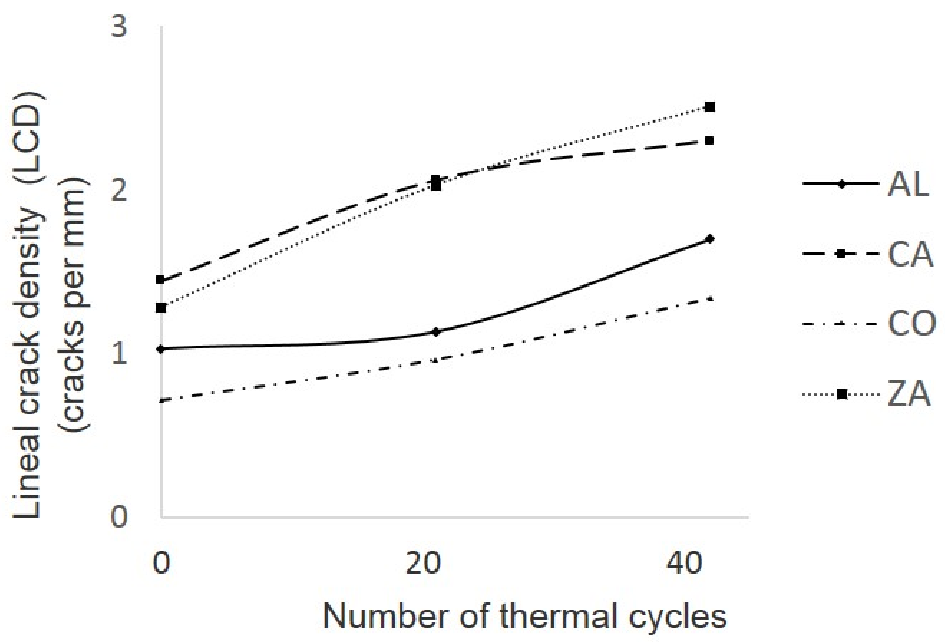

Fig. 6. Variation in linear crack density (LCD) during the thermal test; AL: Alpedrete granite, CA: Cadalso de los Vidrios granite, CO: Colmenar Viejo granite, ZA: Zarzalejo granite

The data in Table 5 show the thermal test-induced proliferation of inter- and intra-microcracks in the Qz, K-Fsp, Pl and Bt crystals in the granites studied.

In AL, K-Fsp had the highest percentage of initial microcracks, followed by Qz, Pl and Bt. The steepest rise in thermal microcracking was observed in K-Fsp, followed by Pl, Qz and Bt.

In CA, Qz had the highest percentage of initial microcracks, followed by Pl, K-Fsp and Bt.

In CO, Qz had the highest percentage of initial microcracks, followed by K-Fsp, Pl and Bt. The rise in microcracking due to thermal change affected the minerals in the following order: K-Fsp > Pl > Qz > Bt.

In ZA, Qz had the highest percentage of initial microcracks, followed by Pl, K-Fsp and Bt. After thermal treatment, microcracking increased most steeply in Pl, followed by Bt, K-Fsp and Qz.

The microscopic analysis of the thin sections prior to the thermal test showed that the four granites began the test with a larger number of inter- than intracrystalline microcracks. As the thermal test progressed, more intracrystalline microcracks appeared and after 42 cycles, all the stones had more intra- than inter-crystalline microcracks. The highest inter- to intracrystalline microcrack ratio was observed in CA, followed by CO, ZA and AL. Granites CO and CA ended the test with a ratio of 1.6, and AL and ZA with 1.1.

Transcrystalline microcracking was infrequent throughout the thermal test.

Table 5. Number of inter- and intra-crystalline microcracks (MC) in 110 linear mm before thermal testing and after 21 and 42 thermal cycles by type of crystal affected

Granite	Before Thermal test						Cycle 21 Thermal test						After TS test						Δ (%)
	Mineral	No. MC	MC type	No. MC	MC type	No. MC	Mineral	No. MC	MC type	No. MC	MC type	No. MC	Mineral	MC	MC type	No. MC	MC type	No. MC	
AL	Qz	162	Inter	102	inter-	365	Qz	169	Inter	107	inter-	520	Qz	207	Inter	133	inter-	631	
			Intra	60					Intra	62					Intra	73			27.4
	K-Fsp	232	Inter	160			K-Fsp	392	Inter	256			K-Fsp	560	Inter	272			
			Intra	72					Intra	136					Intra	288			141.4
	Pl	120	Inter	71	intra-	189	Pl	218	Inter	133	intra-	299	Pl	369	Inter	178	intra-	576	
			Intra	49					Intra	84					Intra	191			207.4
	Bt	40	Inter	32			Bt	40	Inter	24			Bt	72	Inter	48			
			Intra	8					Intra	16					Intra	24			80.0
CA	Qz	300	Inter	245	inter-	649	Qz	338	Inter	248	inter-	736	Qz	353	Inter	255	inter-	825	
			Intra	55					Intra	90					Intra	98			17.4
	K-Fsp	208	Inter	165			K-Fsp	345	Inter	196			K-Fsp	384	Inter	220			
			Intra	43					Intra	149					Intra	165			84.9
	Pl	212	Inter	165	intra-	195	Pl	333	Inter	192	intra-	455	Pl	333	Inter	200	intra-	511	
			Intra	47					Intra	141					Intra	149			57.4
	Bt	125	Inter	75			Bt	175	Inter	100			Bt	250	Inter	150			
			Intra	50					Intra	75					Intra	100			100.0
CO	Qz	158	Inter	100	inter-	411	Qz	182	Inter	111	inter-	483	Qz	200	Inter	121	inter-	523	
			Intra	58					Intra	71					Intra	79			26.6
	K-Fsp	90	Inter	63			K-Fsp	161	Inter	102			K-Fsp	227	Inter	125			
			Intra	27					Intra	59					Intra	102			152.2
	Pl	122	Inter	86	intra-	136	Pl	157	Inter	110	intra-	192	Pl	247	Inter	125	intra-	318	
			Intra	35					Intra	47					Intra	122			103.2
	Bt	46	Inter	31			Bt	46	Inter	31			Bt	46	Inter	31			
			Intra	15					Intra	15					Intra	15			0.0
ZA	Qz	314	Inter	217	inter-	572	Qz	411	Inter	240	inter-	645	Qz	457	Inter	246	inter-	696	
			Intra	97					Intra	171					Intra	211			45.5
	K-Fsp	189	Inter	131			K-Fsp	291	Inter	124			K-Fsp	313	Inter	153			
			Intra	58					Intra	167					Intra	160			65.4
	Pl	234	Inter	160	intra-	230	Pl	389	Inter	217	intra-	526	Pl	446	Inter	217	intra-	640	
			Intra	74					Intra	171					Intra	229			90.2
	Bt	64	Inter	64			Bt	80	Inter	64			Bt	120	Inter	80			
			Intra	0					Intra	16					Intra	40			87.5

AL: Alpedrete granite; CA: Cadalso de los Vidrios granite; CO: Colmenar Viejo granite; ZA: Zarzalejo granite; Δ: variation; Bt: biotite-group minerals; K-Fsp: potassium feldspar; Qz: quartz, Pl: plagioclase

4 Discussion

The pre- and post-cycle petrophysical and petrographic properties (especially) showed that pre-existing microcracks coalesced and new microcracks were generated as decay progressed (Figure 5).

The PM + FM micrographs of the mosaics were essential to quantifying both the pre-existing microcracks and the ones generated. Their analysis led to an understanding of the mechanisms generating decay, such as coalescence of pre-existing microcracks and the development of new unconnected intracrystalline microcracks inside Qz, K-Fsp, Pl and Bt crystals. Thermal expansion is directly proportional to mineral size and also depends on crystal shape, orientation and anisotropy (Ollier, 1984; Warke et al., 1996; Gómez-Heras et al., 2006a, 2008; Vázquez et al., 2010, 2015). ZA, for instance, with larger oriented minerals than the other three granites studied, exhibited the most intense microcracking.

In Qz, pre-existing intracrystalline microcracks appeared in different directions due to the lack of cleavage or twinning in this mineral (Figure 7).

Both K-Fsp and Pl crystals exhibited two right-angled cleavage planes. Cleavage was perfect along plane (001) and good along plane (010). Microcrack inter- and intracrystalline propagation in feldspar (K-Fsp and Pl) is largely governed by its microtexture, in turn the outcome of mineral phase exsolution, for instance, and the respective planes of weakness: macles, cleavage, perthites or pre-existing microcracks. CO, with a larger crystal size than AL and more perthites and macles in its K-Fsps (Figure 7), exhibited a steeper rise in K-Fsp intracrystalline microcracking (271 % versus 186 % in AL), which ran in the same direction as the macles and perthites.

Microcrack propagation in plagioclases is conditioned by their chemical composition and high degree of alteration. Compositional zoning in this mineral may potentially generate porosity in Ca-high crystal interiors due to the ready alterability of their nuclei (Catlos et al., 2011). That zone decayed during the test, generating microcracks that propagated from there to the rest of the crystal. Microcracks also commonly run parallel in the direction of the edges in perthitic textures.

In biotite grains, the planes of basal cleavage split along axis c due to expansion and contraction (Figure 7), leading to concentrated stress and strain along the edges of the crystal (Vázquez et al., 2015) that affected the surrounding minerals.

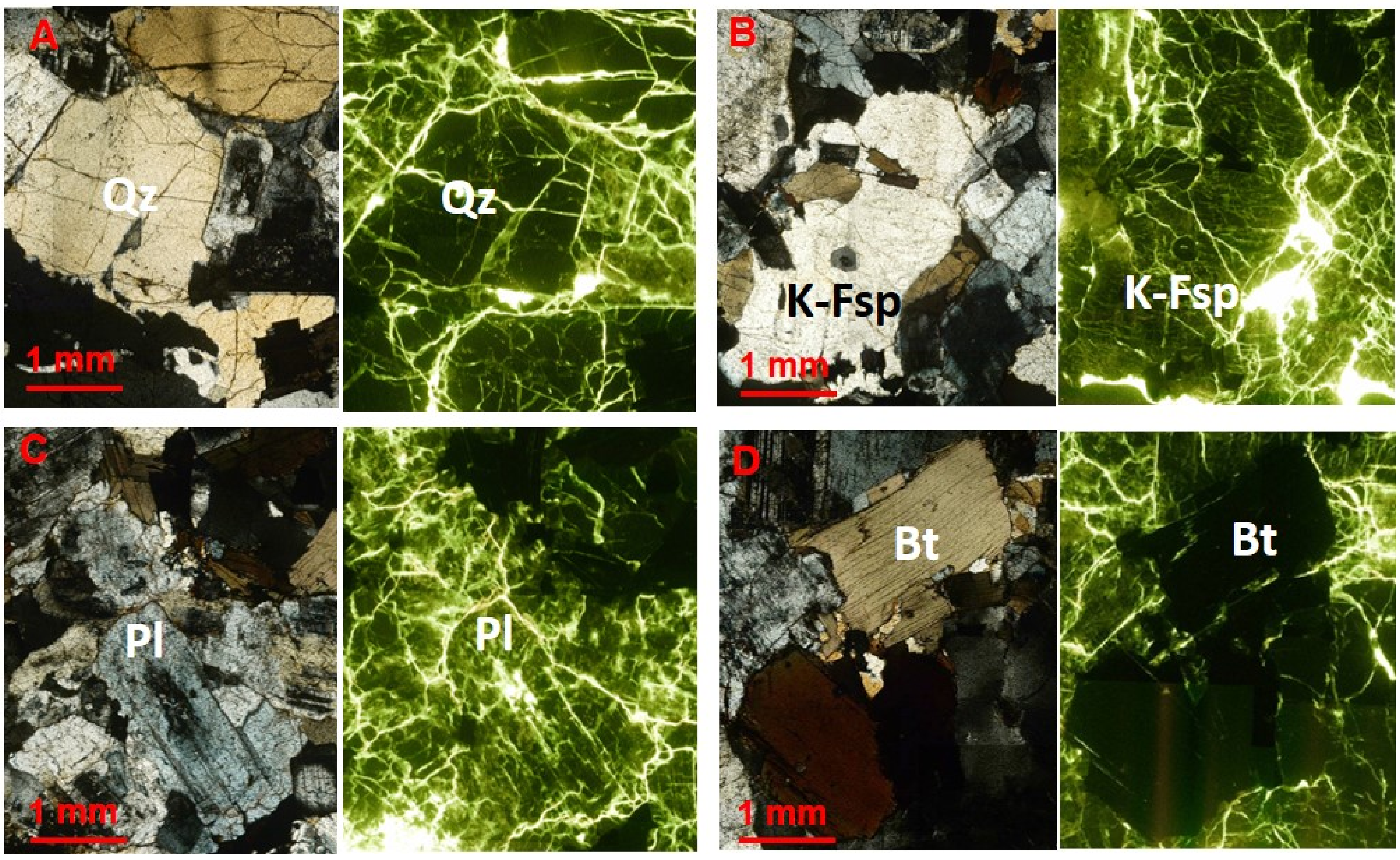

Fig. 7. Micrographs of Zarzalejo granite exposed to 42 thermal cycles: left, PM (crossed Nicols); right, FM; quartz (Qz), potassium feldspar (K-Fsp), plagioclases (Pl) and biotite-group minerals (Bt)

LCD indicated that inter-, intra- and transcrystalline microcracking varied in the minerals in each granite. In the present study, the ratio of inter- to intra-crystalline microcracks depended largely on rock texture and mineralogy (Table 5). CA, which had the smallest size minerals, had a higher ratio than ZA, which bears larger minerals. The decline in this ratio as the thermal cycles progressed was an indication that microcracks developed more intensely inside the crystals.

Another aspect to be borne in mind is that ZA has more oriented crystals (Freire-Lista et al., 2015d). Adjacent crystals oriented along the expansion axis generate anisotropy as they expand in the same direction, creating higher pressure areas where more microcracks may arise. The more oriented a stone's crystals, then, the more intense is its decay with thermal cycles.

The proportion of intercrystalline microcracks was especially high at the Qz-Qz, and Qz-K-Fsp and Qz-Pl boundaries, much lower between feldspars (K-Fsp-K-Fsp, Pl-Pl and Pl-K-Fsp) and even lower across the boundaries of the biotite-group minerals. As observed in other granites (Wang et al., 1989; Lin, 2002), this was due to the fact that the thermal expansion coefficient for Qz is substantially higher than for K-Fsp and Pl (Skinner, 1966).

As the MIP analyser used operated at 0.001 μm to 400 μm, it was unable to detect larger diameter pores. The thermal test induced a small rise, on the order of hundredths of a percentage point, in Pe in the four granites due to the appearance of microcracks. The highest Pe was observed in ZA, the most intensely weathered of the granites studied, which also had the highest final MIP value.

The porosity values found with Pe and MIP were very similar, although the former were somewhat higher, with one exception: in CA granite the final MIP was higher than the final *Pe* value, an indication that the microcrack size after thermal treatment was under 400 μm and that in this granite, most of the newly generated microcracks were under 5 μm. In other words, the pre-existing microcracks did not widen but rather may have coalesced, while new microcracks appeared.

MIP revealed that the thermal test induced a steeper rise in macroporosity than in microporosity in AL and ZA. Inasmuch as the Pl crystals observed in these granites had nuclei exhibiting sericite alterations that may have been washed out by the cooling water, larger pores would form in these than in the other two stones (Figure 7).

MIP values remained essentially unaltered in CO. Microporosity grew in this granite because decay increased the size of its microcracks, although not to above the 5 μm macroporosity threshold. Its macroporosity in fact declined. The chemical alteration of plagioclases and potassium feldspars (Taboada and García, 1999) by the thermal test favoured the formation of microparticles that may have been carried to the pores by any water present, reducing pore size. The decline in macroporosity observed may have also been an instrumental artefact, however, for pores with diameters greater than 400 μm would lie outside the range detectable by MIP (Figure 4). CO, along with ZA, exhibited the steepest rise in effective porosity. That rise was related to the increase in LCD during thermal cycle-induced decay.

The mean V_p declined by 6 % to 7 % for AL, CA and ZA. Despite the high standard deviation this decline is an indication of a trend toward lower V_p values after thermal cycles. A clear downturn was observed in V_s, where the difference in the pre- and post- heating values was much greater than the standard deviation in all the types of granite except ZA, which exhibited the lowest V_s.

In the present study, E_{dyn} declined slightly but remained high in all the granites after the thermal test. $E_{final}/E_{initial}$ ratios ranging from 0.87 to 0.94 were found (in CA and CO, respectively), an indication that the test deployed here caused no severe internal damage, although E_{dyn} was affected by the slight proliferation of microcracking observed.

ZA, with the largest feldspars and largest number of initial microcracks (LCD), had low V_p and V_s values. It was also the granite with the lowest pre- and post-test E_{dyn}. CO exhibited the highest pre- and post-test E_{dyn} due to its lower LCD and Pe and higher pre- and post-test V_p than the other three granites. E_{dyn} was low in CA because of the large numbers of intercrystalline microcracks in this granite. Moreover, the microcrack proximity attendant upon a smaller crystal size would generate a lower E_{dyn}. While the relative decline in E_{dyn} was smallest in CA, it had the lowest $E_{final}/E_{initial}$ ratio, possibly as a result of the smaller increase in its LCD, for its $LCD_{final}/LCD_{initial}$ ratio was smaller than in the other three stones.

CA, a leucogranite, was found to have higher initial L* and WI values due to its lower mica content. The ΔE* values recorded revealed slight post-test variations in colour in all four granites that would have been extremely difficult to detect with the naked eye.

Parameter b* rose most in CO, with a shift toward slightly more yellow tones, perhaps as an outcome of the alteration of its biotites and feldspars due to the early stage diffusion of thermally oxidised Fe^{2+} through the microcracks. That would have caused some dying and a rise in YI. As CA had more biotite-group minerals, it was the granite exhibiting the lowest ΔE*.

In this study L was observed to decline after the thermal cycles. ZA exhibited lower initial surface hardness due to its greater initial porosity, the larger size of its K-Fsp and Pl crystals and its more numerous intracrystalline Qz microcracks. Surface hardness declined more in ZA than in the other granites after thermal treatment due to its greater post-test LCD.

4 Conclusions

The initial and final condition of the specimen, its petrographic (composition, texture and microestructurea) and petrophysical properties must be ascertained to understand thermal decay mechanisms in granite.

The use of polarising petrographic and fluorescence microscopic techniques to study the development of microcracks in four building granites lent insight into the objective variation in the petrophysical parameters of these materials after 42 thermal cycles (20 °C to 105 °C). The technique proved to be very useful for choosing granites apt for use as building materials in environments and climates characterised by thermal stress. The declines in ρb, V_p, V_s, E_{st}, L and the rises in Pe and MIP values observed in the microscope images of the granites denoted the coalescence of pre-existing and the generation of new, primarily intracrystalline microcracks.

Nonetheless, the fairly minor changes observed in the petrophysical properties of the granite before and after heat treatment attested to its thermal durability within the temperature range tested. Ultrasonic wave velocity, which assessed decay most accurately, yielded the widest variation in the properties analysed. In contrast, microscopic observation furnished valuable information on the behaviour of each mineral during microcracking, determining the decay mechanism more accurately in granites that exhibited scantly varying petrophysical properties.

Intracrystalline microcracking was more intense in K-Fsp and Pl and less so in Qz and Bt. Qz exhibited mainly intragranular microcracks with irregular cracking patterns. In feldspars, the microcracks ran across altered areas, including macles, perthites and cleavage planes. Greater decay and concentrated microcracking were observed at the centre of highly calcareous, zoned plagioclases. In K-Fsp, in turn, microcracking tended to develop in the direction of macles, cleavage planes or the edges of perthites. Microcracks propagated along the cleavage planes in biotite-group minerals.

Ultrasound findings corroborated the existence of the microcracking detected with other techniques and determined granite durability. LCD rose with the number of thermal cycles. All four granites had a high E_{dyn} before and after the 42 cycles and showed no significant colour change after the test.

#

CA and CO were the most thermal cycle-resistant of the four granites studied. ZA was the lowest quality and lowest thermal-resistant stone. It also had the highest LCD and Pe and the lowest V_p, L and E_{dyn}. Inasmuch as it also housed the largest and most numerous K-Fsp particles, it should be used with caution as a building material.

Overall, these stones performed well under the thermal test, with scant variation in their petrophysical properties, thanks primarily to their high initial ρb, V_p, V_s, E_{dyn}, L and low initial Pe, MIP and LCD values.

The ability to predict (de novo or restoration) building granite behaviour in climates or sites characterised by temperature change will help choose the most suitable material and prevent surface microcracking, which favours the frequent appearance of surface crystal disintegration and detachment, as well as façade scaling and flaking. Inasmuch as thermally-induced decay affected the granite surface, the petrophysical properties of the stone as a whole scantly varied. Microcracking, which is perfectly visible under a microscope, is the form of decay prompted by temperature fluctuations. These microcracks may develop over time, ultimately impacting the petrophysical properties and hence the quality and durability of the material.

Acknowledgments

This study was funded by the Community of Madrid under the GEOMATERIALS-2CM Program (S2013/MIT-2914). The authors are members of the Complutense University of Madrid's Research Group: "Alteración y Conservación de los Materiales Pétreos del Patrimonio" (ref. 921349). The authors wish to thank the Geological and Mining Institute of Spain for conducting the thermal tests. The petrophysical assessments were run at the IGEO Petrophysical Laboratory, affiliated with the Moncloa Campus of International Excellence (UCM-UPM) Heritage Laboratory Network (RedLabPat). The assistance, input and support provided by laboratory technicians Pedro Lozano, Marian Barajas and Carmen Valdehita are gratefully acknowledged. Manuscript edited by Margaret Clark, professional translator and English language science editor.

References

Alm, O., Jaktlund L.L and Kou, S. 1985. The influence of microcrack density on the elastic and fracture mechanical properties of Stripa granite. Physics of the Earth and Planetary Interiors. 40(3), 161–179.

Åkesson, U., Hansson, J., Stigha, J. 2004. Characterisation of microcracks in the Bohus granite, western Sweden, caused by uniaxial cyclic loading. Engineering Geology. 72, 131–142.

Anders, M.H, Laubach, S.E., Scholz, C.H., 2014. Microfractures: A review. Journal of Structural Geology. 69, 377–394.

Akesson, U., Stigh, J., Lindqvist, J.E. and Göransson, M., 2003. The influence of foliation on the fragility of granitic rocks, image analysis and quantitative microscopy. Engineering Geology. 68, 275–88.

Aoki, H. and Matsukura, Y., 2007. A new technique for non-destructive field measurement of rock-surface strength: an application of the Equotip hardness tester to weathering studies. Earth Surface Processes and Landforms. 32, 1759–1769.

Aoki H. and Matsukura Y. 2008. Estimating the unconfined compressive strength of intact rocks from Equotip hardness. Bulletin of Engineering Geology and the Environment. 67(1), 23–29.

Benavente, D., Martínez-Martínez, J., Jáuregui, P., Rodríguez, M.A. and García del Cura, M.A., 2006. Assessment of the strength of building rocks using signal processing procedures. Construction and Building Materials. 20, 562–568.

Brotóns Torres, V., Tomás Jover, R., Ivorra, S. and Alarcón J.C., 2013. Temperature influence on the physical and mechanical properties of a porous rock: San Julian's calcarenite. Engineering Geology. 167, 117–127.

Caballero, J.M, González Casado, J.M., Casquet, C., Galindo, C. and Tornos, E., 1996. Episienitas de la Sierra de Guadarrama: un proceso hidrotermal regional de edad Pérmico Inferior ligado al inicio de la extensión alpina. Cuadernos de Geología ibérica 20 183-201. Servicio de Publicaciones. Universidad Complutense. Madrid.

Catlos, E., Baker, C., Sorensen S., Jacob, L. and Çemen, I., 2011. Linking microcracks and mineral zoning of detachment-exhumed granites to their tectonomagmatic history: Evidence from the Salihli and Turgutlu plutons in western Turkey (Menderes Massif). Journal of Structural Geology. 33, 951–969.

Chaki, S., Takarli, M. and Agbodjan, W.P., 2008. Influence of thermal damage on physical properties of a granite rock: porosity, permeability and ultrasonic wave evolutions. Construction and Building Materials. 22, 1456–1461.

Chen, Y, Kobayashi, T., Kuriki, Y., Kusuda, H. and Mabuchi M. 2008. Observation of microstructures in granite samples subjected to one cycle of heating and cooling. Journal of the Japan Society of Engineering Geology. 49(4), 217–26.

Christaras, B., Auger, F. and Mosse, E., 1994. Determination of the moduli of elasticity of rocks. Comparison of the ultrasonic velocity and mechanical resonance frequency methods with direct static methods. Materials and Structures. 27, 222–228.

Darracott, B.W. and Orr, C.M., 1976. Geophysics and rock engineering. Symp. On Exploration for Rock Engineering. Johannesburg. 1, 159–164. Cape Town/Rotterdam: Balkema.

Dearman, W.R., Baynes, F.J. and Irfan, T.Y., 1978. Engineering geology of weathered granite. Engineering Geology 12, 345–374.

Demirdag S., 2013. Effects of freezing–thawing and thermal shock cycles on physical and mechanical properties of filled and unfilled travertine. Construction and Building Materials. 47, 1395–1401.

De la Torre, R., Sancho, L., Horneck, G., de los Ríos, A., Wierzchos, J., Olsson-Francis, K., Cockell, C., Rettberg, P., Berger, T., De Vera, J.P., Ott, S., Martinez-Frías, J., González-Melendi, P., Mercedes-Lucas, M., Reina, M., Pintado, A., Demets, R., 2010. Survival of lichens and bacteria exposed to outer space conditions – Results of the Lithopanspermia experiments. Icarus. 208, 735–748.

De Vicente, G., Vegas, R., Muñoz Martín, A., Silva, P.G., Andriessen, P., Cloetingh, S., González Casado, J.M., Van Wees, J.D., Álvarez, J., Carbó, A. and Olaiz, A., 2007. Cenozoic thick-skinned deformation and topography evolution of the Spanish Central System. Global and Planetary Change. 58, 335–381.

Dwivedi, R.D., Goel, R.K., Prasad, V.V.R., Amalendu Sinha, 2008. Thermo-mechanical properties of Indian and other granites. International Journal of Rock Mechanics and Mining Sciences. 45, 303–315.

Erguler, Z.A. and Shakoor. A., 2009. Relative contribution of various climatic processes in disintegration of clay-bearing rocks. Engineering Geology. 108, 36–42.

Fort, R., Alvarez de Buergo, M., Perez-Monserrat, E., Varas, M.J., 2010. Monzogranitic batholiths as a supplying source for the heritage construction in the northwest of Madrid. Engineering Geology. 115, 149–157. doi:10.1016/j.enggeo.2009.09.001.

Fort, R., Varas, M.J., Alvarez de Buergo, M. and Freire, D.M., 2011. Determination of anisotropy to enhance the durability of natural stone. Journal of Geophysics and Engineering. 8, 132–144.

Fort, R., Alvarez de Buergo, M., Perez-Monserrat, E., Gómez-Heras, M., Varas, M.J. and Freire, D.M., 2013. Evolution in the use of natural building stone in Madrid, Spain. Quarterly Journal of Engineering Geology and Hydrogeology. 46 (4), 421–429.

Franzoni, E., Sassonia, E., Scherer, G.W., Naidu, S., 2013. Artificial weathering of stone by heating. Journal of Cultural Heritage. 14, 85–93.

Fredrich, J.T. and Wong T.F., 1986. Micromechanics of thermally induced cracking in three crustal rocks. Journal of Geophysical Research. 91, 743–64.

Freire-Lista, D.M., Fort, R., Varas-Muriel, M.J. 2015a. Freeze-thaw fracturing in building granites. Cold Regions Science and Technology 113, 40–51. Doi: 10.1016/j.coldregions.2015.01.008.

Freire-Lista, D.M., Fort, R., Varas-Muriel, M.J., 2015b. Alpedrete granite (Spain). A nomination for the "Global Heritage Stone Resource" designation. Episodes. 38 (2), 1–8.

Freire-Lista, D.M., Fort, R., Varas-Muriel, M.J., 2015c. Nomination of Zarzalejo granite, a Spanish heritage building stone, as a "Global Heritage Stone Resource". Energy Procedia. 76, 642–651.#

Freire-Lista, D.M., Gomez-Villalba, L.S., Fort, R., 2015d. Microcracking of granite feldspar during thermal artificial processes. Periodico di mineralogia. 84, 83–95.

Freire-Lista, D.M., and Fort, R., 2015. The Piedra Berroqueña region: candidacy for Global Heritage Stone Province status. Geoscience Canada. https://journals.lib.unb.ca/index.php/GC/issue/view/1603.#

Gale, J., Landerb, R., Reeda, R., Laubach, S., 2010. Modeling fracture porosity evolution in dolostone. Journal of Structural Geology. 32, 1201–1211.

García-del-Cura, M.A., Benavente, D., Bernabéu, A. and Martínez-Martínez, J., 2008. The effect of surface finishes on outdoor granite and limestone pavers. Materiales de Construcción. 58, 289-290, 65-79, ISSN: 0465-2746 eISSN: 1988–3226.

Gokceoglu, C., Zorlu, K., Ceryan, S. and Nefeslioglu, H.A., 2009. A comparative study on indirect determination of degree of weathering of granites from some physical and strength parameters by two soft computing techniques. Materials Characterization. 60, 1317–1327.

Gómez-Heras, M., Smith, B.J. and Fort, R., 2006. Surface temperature differences between minerals in crystalline rocks: implications for granular disintegration of granites through thermal fatigue. Geomorphology. 78, 236–249.

Gómez-Heras, M., 2006. Procesos y formas de deterioro térmico en piedra natural del patrimonio arquitectónico. Editorial Complutense, Madrid. 367 pp. ISBN 84-669-2801-4.

Gómez-Heras, M., Smith, B.J. and Fort, R., 2008. Influence of surface heterogeneities of building granite on its thermal response and its potential for the generation of thermoclasty. Environmental Geology. 56, 547–560.

Gómez-Heras, M., Stephen, M., Smith, B.J. and Fort, R., 2009. Impacts of fire on Stone-Built Heritage. An Overview. Architectural Conservation. 2, 15, 47–58.

Gómez-Moreno, G., Lombardero, M., Regueiro y Gonzalez-barros, M., 1995. Study of the granites of the autonomous comunity of Madrid. Instituto Geológico y Minero de España, Madrid, Spain. (In Spanish)

Gräf, V., Jamek, M., Rohatsch, A. and Tschegg, E., 2013. Effects of thermal-heating cycle treatment on thermal expansion behavior of different building stones. Rock Mechanics & Mining Sciences. 64, 228–235.

Hale, P.A. and Shakoor, A., 2003. A laboratory investigation of the effects of cyclic heating and cooling, wetting and drying, and freezing and thawing on the compressive strength of selected sandstones. Environmental and Engineering Geoscience. 9, 117–130.

Hall, K., 1999. The role of thermal stress fatigue in the breakdown of rock in cold regions. Geomorphology. 31, 47–63.

Hall, K. and Thorn, E., 2014. Thermal fatigue and thermal shock in bedrock: An attempt to unravel the geomorphic processes and products. Geomorphology. 206, 1–13.

Halsey, D. P. Mitchell, D. J. and Dews, S. J., 1998. Influence of climatically induced cycles in physical weathering Quarterly Journal of Engineering Geology. 31, 359–367.

Heuze, F.E., 1983. High-temperature mechanical, physical and thermal properties of granitic rocks—a review. International Journal of Rock Mechanics and Mining Sciences. 20 (1), 3–10.

Homand-Etienne, F., Troalen, J.P., 1984. Behaviour of granites and limestones subjected to slow and homogeneous temperature changes. Engineering Geology. 20 (3), 219–233.

Homand-Etienne H, Houpert R., 1989. Thermally induced micro-cracking in granites: characterization and analysis. International Journal of Rock Mechanics and Mining Sciences. Abstr. 26, 125–34.

Inserra, C., Biwa, S. and Chen, Y., 2013. Influence of thermal damage on linear and nonlinear acoustic properties of granite. International Journal of Rock Mechanics and Mining Sciences. 62, 96–104.

Iñigo, A.C., Vicente, M.A., Rives, V., 2000. Weathering and decay of granitic rocks: its relation to their pore network. Mechanics of Materials. 32, 555–560.

Iñigo, A.C., García-Talegón, J., Vicente-Tavera, S., Martín-González, S., Casado-Marín, S., Vargas-Muñoz, M., Pérez-Rodríguez, J.L., 2013. Colour and ultrasound propagation speed changes by different ageing of freezing/thawing and cooling/heating in granitic materials. Cold Regions Science and Technology. 85, 71–78.

Ismael, I. S. and Hassan, M.S., 2008. Characterization of some Egyptian serpentinites used as ornamental stones. Chinese Journal of Geochemistry. 27, 140–149.

Kern, H., Liu, B. and Popp, T., 1997. Relationship between anisotropy of P and S wave velocities and anisotropy of attenuation in serpentinite and amphibolite. Journal of Geophysical Research. 102, 3051–65.

Kawasaki, S., Tanimoto, C., Koizumi, K., Ishikawa, M., 2002. An attempt to estimate mechanical properties of rocks using the Equotip Hardness tester. Journal of Japan Society of Engineering Geology. 43, 244–248.

Kawasaki, S., Kaneko, K., 2004. Estimation method for weathering thickness of man-made weathering rocks by using the Equotip hardness Tester. Proceedings of the ISRM Regional Symposium EUROROCK 2004 and 53rd Geomechanics Colloquy, Salzburg 491–494.

Laubach, S.E., 1997. A Method to Detect Natural Fracture Strike in Sandstones. AAPG Bulletin. 81 (4), 604–623.

Lin, W., Takahashi, M. and Sugita, N., 1995. Change of microcrack widths induced by temperature increase in Inada granite. Journal of the Japan Society of Engineering Geology. 36, 300–304.

Lin, W., 2002. Permanent strain of thermal expansion and thermally induced microcracking in Inada granite. Journal of geophysical research. 107(B10), 1–16.

Mambou, L.L.N., Ndop, J., Bienvenu, J.M., 2015. Modeling and numerical analysis of granite rock specimen under mechanical loading and fire. Journal of Rock Mechanics and Geotechnical Engineering. 7(1), 101–108.

Mejías, M., Renard, P., Glenz, D., 2009. Hydraulic testing of low-permeability formations. A case study in the granite of Cadalso de los Vidrios, Spain. Engineering Geology. 107, 88–97.

Miskovsky, K., Taborda Duarte, M., Kou, S.Q. and Lindqvist, P.A., 2004. Influence of the mineralogical composition and textural properties on the quality of coarse aggregates. Journal of Materials Engineering and Performance. 13, 144–50.

Moses, C., Robinson, D. and Barlow, J., 2014. Methods for measuring rock surface weathering and erosion: A critical review. Earth-Science Reviews. 135, 141–161.

Murphy, W., Smith, J.D. and Inkpen, R.J., 1996. Errors associated with determining P and S acoustic wave velocities for stone weathering studies. In: Smith, B.J., Warke, P.A. (Eds.), Processes of Urban Stone Decay, Donhead, London, pp. 228–244.

Nasseri, M.H.B., Schubnel, A. and Young R.P., 2007. Coupled evolutions of fracture toughness and elastic wave velocities at high crack density in thermally treated Westerly granite. International Journal of Rock Mechanics and Mining Sciences. 44, 601–616.

Ollier, C.D., 1984. Weathering. Geomorphology Texts, vol. 2. Longman, London. 270 pp.

Ozcelik, Y., Careddu, N. and Yilmazkaya, E., 2012. The effects of freeze–thaw cycles on the gloss values of polished stone surfaces. Cold Regions Science and Technology. 82, 49–55.

Pires, V, Rosa LG and Dionísio, A., 2014. Implications of exposure to high temperatures for stone cladding requirements of three Portuguese granites regarding the use of dowel–hole anchoring systems. Construction and Building Materials. 201 (64), 440–450.

Raisanen, M., 2004. Relationships between texture and mechanical properties of hybrid rocks from the Jaala-Iitti complex, southeastern Finland. Engineering Geology. 74, 197–211.

Reuschlé, T, Haore, S.G, Darot, M., 2006. The effect of heating on the microstructural evolution of La Peyratte granite deduced from acoustic velocity measurements. Earth and Planetary Science Letters. 243, 692–700.

Rivas, T., Pozo, S., Fiorucci, M.P. López, A.J., Ramil, A., 2012. Nd: YVO4 laser removal of graffiti from granite. Influence of paint and rock properties on cleaning efficacy. Applied Surface Science. 263, 563–572.

Rodríguez, C., Sebastián, E., 1994. Técnicas de análisis del sistema poroso de materiales pétreos ornamentales: usos y limitaciones. Ing. Civil 96, 130–142.

Russel, S.A., 1927. Stone preservation committee report (Appendix I). H.M. Stationary Office, London.

Sajid, M., Coggan, J., Arif, M., Andersen, J., Rollinson, G., 2016. Petrographic features as an effective indicator for the variation in strength of granites. Engineering Geology, doi: 10.1016/j.enggeo.2016.01.001.

Scarciglia, F., Saporito, N., La Russa, M.F., Le Pera, E., Macchione, M., Puntillo, D., Crisci, G.M., Pezzino, A., 2012. Role of lichens in weathering of granodiorite in the Sila uplands (Calabria, southern Italy) Sedimentary Geology 280, 119–134.

Schiavon, N., Chiavari, G., Schiavon, G., Fabbri, D., 1995. Nature and decay effects of urban soiling on granitic building stones. The Science of the Total Environment. 167, 87–101.

Schubnel, A., Benson, P.M., Thompson, B.D., Hazzard, J.F. and Young, R.P., 2006. Quantifying damage, saturation and anisotropy in cracked rocks by inverting elastic wave velocities. Pure and Applied Geophysics. 163, 947–73.

Seo, Y.S., Jeong, G.C., Kim, J.S., Ichikawa, Y., 2002. Microscopic observation and contact stress analysis of granite under compression. Engineering Geology. 63, 259–275.

Shao, S., Wasantha, P.L.P., Ranjith, P.G. and Chen, B.K., 2014. Effect of cooling rate on the mechanical behavior of heated Strathbogie granite with different grain sizes. International Journal of Rock Mechanics and Mining Sciences. 70, 381–387.

Siegesmund, S., Dürrast H (2011) Physical and mechanical properties of rocks. In: Siegesmund S, Snethlage, R. (eds) Stone in architecture—properties, durability, 4th edn. Springer, Berlin, pp 97–226

Siegesmund, S., Török, A., 2011. Building stones. In: Siegesmund S, Snethlage R (eds) Stone in architecture-properties, durability, 4th edn. Springer, Berlin, pp 11–96.

Simmons, G. and Cooper, H.W., 1978. Thermal cycle cracks in three igneous rocks. International Journal of Rock Mechanics and Mining Sciences, Geomech Abstract. 15, 145–8.

Skinner, B.J., 1966. Thermal expansion. In Handbook of physical constants. Geological Society of America Memoirs. 97, 75–96.

Smith, B.J., Srinivasan, S., Gómez-Heras, M., Basheer, P.A.M. and Viles, H.A., 2011. Near-surface temperature cycling of stone and its implications for scales of surface deterioration. Geomorphology. 130, 76–82.

Sousa, L.M.O., Suarez del Rio, L.M., Calleja, L., Ruiz de Argondona, V.G. and Rey, A.R., 2005. Influence of microcracks and porosity on the physico-mechanical properties and weathering of ornamental granites. Engineering Geology. 77, 153–168.

Sousa, L.M.O., 2014. Petrophysical properties and durability of granites employed as building stone: a comprehensive evaluation. Bulletin of Engineering Geology and the Environment. 73, 569–588.

Svahn, H., 2006. Non-Destructive field Tests in Stone Conservation: Literature Study. Rapport från Riksantikvarieämbetet, Stockholm. 63 pp.

Taboada, T., García, C., 1999. Pseudomorphic transformation of plagioclases during the weathering of granitic rocks in Galicia NW Spain. Catena. 35, 291–302.

Takarli, M., Prince, W. and Siddique, R., 2008. Damage in granite under heating/cooling cycles and water freeze–thaw conditions. International Journal of Rock Mechanics and Mining Sciences. 45, 1164–1175.

Takarli, M. and Prince-Agbodjan, W., 2008. Temperature Effects on Physical Properties and Mechanical Behavior of Granite: Experimental Investigation of Material Damage. Journal of ASTM international. 5 (3), 1–13.

TS EN 14066, Natural stone test methods-determination of resistance to ageing by thermal shock. Institute of Turkish Standards (Türk Standartları Enstitüsü, TSE), p. 3.

Tuğrul, A., Zarif, I.H., 1999. Correlation of mineralogical and textural characteristics with engineering properties of selected granitic rocks from Turkey. Engineering Geology 51, 303–317.

Tuğrul, A., 2004. The effect of weathering on pore geometry and compressive strength of selected rock types from Turkey. Engineering Geology. 75, 215–227.

UNE-EN 771-6, 2012. Specification for masonry units - Part 6: Natural stone masonry units. AENOR. Madrid.

UNE-EN 14066, 2003. Natural stone test methods - Determination of resistance to ageing by thermal shock. AENOR. Madrid.

UNE-EN 14579, 2005. Natural Stone Test Methods - Determination of Sound Speed Propagation. AENOR. Madrid.

UNE-EN 15886, 2011. Conservation of cultural property - Test methods - Colour measurement of surfaces. AENOR. Madrid.

UNE-EN 1936, 2007. Natural Stone Test Methods - Determination of Real Density and Apparent Density and of Total and Open Porosity. AENOR. Madrid.

Upadhyay, D., 2012. Alteration of plagioclase to nepheline in the Khariar alkaline complex, SE India: Constraints on metasomatic replacement reaction mechanisms. Lithos. 155, 19–29.

Vasconcelos, G., Lourenço, P.B., Alves, C.S.A. and Pamplona, J., 2007. Prediction of themechanical properties of granites by ultrasonic pulse velocity and Schmidt Hammer hardness. Proc. 10th North American Masonary Conference, St. Louis, Missouri. 980–991.

Vasconcelos, G., Lourenço, P.B., Alves, C.A.S. and Pamplona, J. 2009. Compressive Behavior of Granite: Experimental Approach. Journal of Materials in Civil Engineering. 21(9), 502–511.

Vázquez, P., 2010. Granitos ornamentales: caracterización, durabilidad y sugerencias de uso. Tesis Doctoral. Universidad de Oviedo. 314 pp.

Vázquez, P., Alonso, F.J. Esbert, R.M. and Ordaz, J., 2010. Ornamental granites: Relationships between p-waves velocity, water capillary absorption and the crack network. Construction and Building Materials. 24, 2536–2541.

Vázquez, P., Shushakova, V., Gómez-Heras, M., 2015. Influence of mineralogy on granite decay induced by temperature increase: Experimental observations and stress simulation. Engineering Geology. 189, 58–67.

Verwaal, W. and Mulder, A., 1993. Estimating rock strength with the Equotip hardness tester. International Journal of Rock Mechanics and Mining Sciences. 30, 659–662.

Viles, H., Goudie, A., Grab, S. and Lalley, J., 2011. The use of the Schmidt Hammer and Equotip for rock hardness assessment in geomorphology and heritage science: a comparative analysis. Earth Surface Processes and Landforms. 36, 320–333.

Villaseca, C., Orejana, D. and Belousova, E.A., 2012. Recycled metaigneous crustal sources for S- and I-type Variscan granitoids from the Spanish Central System batholith: Constraints from Hf isotope zircon composition. Lithos. 153, 84–93.

Warke, P. A., Smith, B. J. and Magee, R. W., 1996. Thermal response characteristics of stone: implications for weathering of soiled surfaces in urban environments. Earth Surface Processes and Landforms. 21, 295–306.

Wang, H. F., Bonner, B. P, Carlson, S. R., Kowallis, B. J. and Heard, H. C. 1989. Thermal stress cracking in granite. Journal of Geophysical Research: Solid Earth. 94, 1745–1758.

Wanne, T.S. and Young, R.P., 2008. Bonded-particle modeling of thermally fractured granite. International Journal of Rock Mechanics and Mining Sciences. 45, 789–799.

Williams, H., Turner F., Gilbert Ch. (1958) - An introduction to the study of rocks in thin sections. W.H. Freeman and company. 406pp.

Yavuz, H., 2011. Effect of freeze–thaw and thermal shock weathering on the physical and mechanical properties of an andesite stone. Bulletin of Engineering Geology and the Environment. 70, 187–92.